

# Stable Numerical Integration of an Epitaxial Growth Model with Slope Selection

Gregory M. Seyfarth

*Department of Physics and Astronomy, Colby College, Waterville, Maine 04901, USA*

Benjamin P. Vollmayr-Lee

*Department of Physics and Astronomy, Bucknell University, Lewisburg, Pennsylvania 17837, USA*

(Dated: March 22, 2013)

We consider a continuum phase field model for molecular beam epitaxial growth with slope selection, with the goal of determining stable numerical time integration methods for the dynamics. We parametrize a class of semi-implicit methods that are linear in the updated field, which allows for efficient implementation with fast Fourier transforms. We perform unconditional von Neumann stability analysis to identify the region of stability in parameter space, and then test these predictions numerically for gradient stability. We find strong agreement between the approaches.

PACS numbers: 05.10.-a, 68.35.Ct, 02.60.Cb

## I. INTRODUCTION

In molecular beam epitaxial (MBE) growth the Ehrlich-Schwoebel effect [1, 2] can destabilize a flat interface and lead to the formation of pyramids or mounds [3]. These surface features then coarsen, with their height and spatial extent growing as powers of time. Theoretical studies of MBE coarsening typically employ continuum models, justified by appeal to the large distance and slow time scales involved. The resulting field equations of motion are nonlinear, and to make progress they must be integrated numerically, a process which, unfortunately, is hampered by numerical instabilities. As such, much recent effort has been devoted to finding stable integration methods. In this work, we derive a class of stable numerical integration methods that are particularly efficient and simple to implement because the updated field can be obtained via the fast Fourier transform (FFT).

The model we consider employs a height field  $h(x, y, t)$  that is a continuous function of space and time, and which obeys the equation of motion

$$\frac{\partial h}{\partial t} = -\nabla^4 h - \nabla \cdot \left\{ (1 - |\nabla h|^2) \nabla h \right\}, \quad (1)$$

applicable for MBE growth with isotropic slope selection. The motivation for this and related models is discussed below. With these dynamics, equilibrated regions of uniform gradient and unit slope form. Domains with different slope orientations meet at edges of constant width, and as the system evolves the edges are healed out, resulting in the growth of the characteristic domain size. For this particular model it has been found from theoretical analysis [4, 5], simulations [5, 6], and rigorous bounds [7] that the characteristic domain size  $L(t)$  grows with time as  $L \sim t^{1/3}$ .

Numerical simulations of coarsening are useful for testing scaling and the predicted growth laws and for measuring properties of the scaling state, such as correlations, growth law amplitudes, autocorrelation functions, and more (see [8] for a coarsening review). But these simulations face several restrictions. To reach the asymptotic

scaling regime, it is necessary to evolve until  $L(t) \gg w$ , where  $w$  is the width of the edges. But the lattice size  $\Delta x$  must be sufficiently smaller than the edge width in order to resolve the edge shape and corresponding line tension. Finally, the system size  $L_{\text{sys}}$  must be large enough that domains can grow into the scaling regime before finite size effects appear. To satisfy this string of conditions,  $\Delta x \ll w \ll L(t) \ll L_{\text{sys}}$ , requires lattices of very large linear size  $L_{\text{sys}}/\Delta x$ , evolved to late times.

For this reason, it is desirable to use integration schemes that are *accuracy*-limited rather than *stability*-limited. Euler integration of Eq. (1) is only stable for time steps  $\Delta t$  smaller than a threshold determined by the lattice spacing. In contrast, an unconditionally stable method, i.e., one with no conditions on  $\Delta t$ , would allow a time step determined by the natural time scale of the dynamics, which turns out to be considerably more efficient. Accuracy considerations require the typical distance traveled by an edge within one step to be held fixed [9, 10], and since the characteristic edge velocity scales as  $v_{\text{edge}} \sim \partial L / \partial t \sim t^{-2/3}$ , this allows a growing time step  $\Delta t \sim t^{2/3}$ . Using  $dt/dn \sim \Delta t$ , where  $n$  is the number of integration steps, it follows that unconditionally stable methods allow accurate evolution with  $t \sim n^3$ , rather than the stability-limited  $t \sim n$ .

Eyre provided a general approach for generating unconditionally stable semi-implicit integration methods, based on a splitting into expansive and contractive terms [11]. Wang, Wang, and Wise used this approach for Eq. (1), as well as an MBE model without slope selection [6], and this approach has now been extended to a second-order in time method [12] and other developments [13–15]. These schemes are *gradient stable*, which means they preserve the energy-decreasing property of the continuous-time equation. However, these Eyre-based schemes have the drawback that usually a nonlinear term must be treated implicitly, requiring an iterative method to find the updated field, and in the worst case no guarantee of convergence or a unique solution. An alternate approach is to restrict consideration to steps with linear implicit terms that can be solved di-

rectly by FFT, determine the range of step parameters that satisfy unconditional von Neumann (UvN) stability, and then test these parameters numerically for gradient stability. This approach yielded stable, direct steps for the Cahn-Hilliard and Allen-Cahn equations [9], and it is the program we follow here for the MBE model.

Our primary results are the following: for the equation of motion, Eq. (1), there exists a class of first order, semi-implicit steps

$$h_{t+\Delta t} = h_t + \Delta t \left[ -\nabla^4 h_t - \nabla \cdot \{ (1 - |\nabla h_t|^2) \nabla h_t \} \right] + b_1 \Delta t \nabla^2 (h_{t+\Delta t} - h_t) + b_2 \Delta t \nabla^4 (h_{t+\Delta t} - h_t) \quad (2)$$

that provides stable numerical integration for appropriate choice of the parameters  $b_1$  and  $b_2$ , as shown in Fig. 1. The results of our UvN stability analysis are presented as shaded regions while our numerical tests of gradient stability are plotted as points. Although UvN stability does not ensure gradient stability, we find that it is very effective in determining the gradient stable regions, both for single- and many-domain systems. The UvN stability conditions plotted here are independent of lattice type or details of the numerical method (e.g., finite difference versus spectral methods). The difference in stability range for the single- and many-domain systems is revealed by the UvN stability analysis, which shows that the most unstable Fourier mode is that with its wavevector oriented with the local slope  $\nabla h$ . In the many-domain system, each mode samples many different slope directions, which acts to suppress the instability for the parameter range  $-1 < b_1 < -1/2$ .

Our results are consistent with Xu and Tang, who proved gradient stability for the parameters  $b_1 < -1$  and  $b_2 = 1$  [16]. Further work by one of us has led to a demonstration of gradient stability for the entire dark gray shaded region of Fig. 1 [17]. This proof will be presented elsewhere, as it is considerably more general than the model considered here, and does not distinguish the single- and many-domain cases captured by the UvN stability analysis.

The remainder of the paper is as follows. In Sec. II we review some of the properties of the model to provide necessary background for subsequent sections. In Sec. III we present the UvN stability analysis, both for single- and many-domain systems. We describe the numerical tests of gradient stability in Sec. IV, as well as providing the details of our finite-difference implementation of Eq. (2). This is followed by a summary in Sec. V.

## II. THE CONTINUOUS TIME MODEL

In this section we provide motivation for the model we are considering and present some of its properties, showing in particular the instability to pyramid formation and the energy decreasing dynamics of the continuous time model.

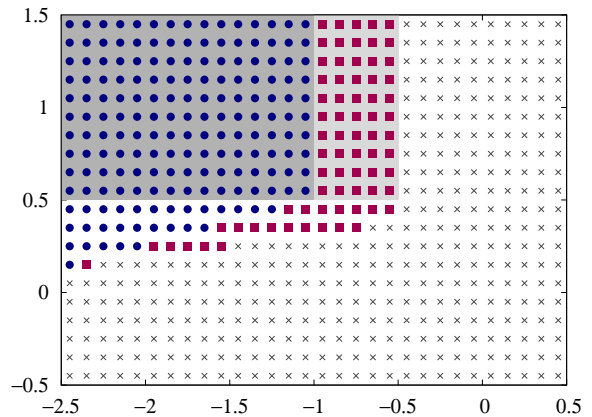


FIG. 1. (color online) Stability diagram for the parameters  $b_1$  and  $b_2$  in Eq. (2). The UvN stable parameter values are shaded in gray, with the darker region corresponding to a single-domain system and the combined gray regions corresponding to a many-domain system. The points represent numerical tests of gradient stability: the (blue) circles are parameter values that are stable for single-domain systems; these together with the (purple) squares are stable for multi-domain systems; and the  $\times$  are parameter values that were found to be unstable.

The height field  $h(x, y, t)$ , is defined in a co-moving frame so that its average is zero, and obeys a continuity equation. The current  $\mathbf{J}$  has an equilibrium surface diffusion contribution equal to the gradient of the local curvature,  $\mathbf{J}_{SD} = \nabla(\nabla^2 h)$  [18], and a non-equilibrium component  $\mathbf{J}_{NE}$ :

$$\frac{\partial h}{\partial t} = -\nabla \cdot \mathbf{J} = -\nabla^4 h - \nabla \cdot \mathbf{J}_{NE}. \quad (3)$$

A noise term is omitted as this is considered to be irrelevant for coarsening [8]. We consider the slope-selecting nonequilibrium current

$$\mathbf{J}_{NE} = (1 - |\nabla h|^2) \nabla h, \quad (4)$$

which gives  $\mathbf{J}_{NE} \sim \nabla h$  for small gradients, an uphill current due to the Ehrlich-Schwoebel effect [3], and  $\mathbf{J}_{NE} = 0$  for slopes of unit magnitude. Inserting Eq. (4) into the continuity equation (3) yields the equation of motion, Eq. (1).

Common variations on this model include slope-selecting currents that vanish for only a discrete set of  $\nabla h$  directions, reflecting the underlying crystalline structure, and models without slope selection. The physical basis and experimental evidence for these various models is described in [4, 5, 19–21] and references therein. Material parameters have been absorbed into rescaling of lateral space dimensions, height, and time.

The equation of motion, Eq. (1), can be written as a gradient flow

$$\frac{\partial h}{\partial t} = -\frac{\delta F}{\delta h} \quad (5)$$

for the free energy functional

$$F[h] = \int d^2x \left\{ \frac{1}{2} (\nabla h)^2 + \frac{1}{4} (1 - |\nabla h|^2)^2 \right\}. \quad (6)$$

Gradient flow results in a monotonically decreasing free energy,

$$\frac{d}{dt} F = \int d^2x \left( \frac{\delta F}{\delta h} \right) \frac{\partial h}{\partial t} = - \int d^2x \left( \frac{\partial h}{\partial t} \right)^2 \leq 0. \quad (7)$$

As first noted by Eyre [11], the essential stability criterion for discrete time steps is to preserve the energy decreasing property of the continuous-time equation. This is known as the gradient stability condition.

Next we review the linear stability of the continuous time equation, which will be useful context for the von Neumann stability analysis in Sec. III. Consider a height field

$$h(x, y, t) = Cx + \eta(x, y, t), \quad (8)$$

which consists of small deviations  $\eta$  from a uniform slope. Inserting this into Eq. (1), linearizing in  $\eta$ , and Fourier transforming to  $\tilde{\eta}(\mathbf{k}, t) \equiv \int d^2x \exp(i\mathbf{k} \cdot \mathbf{x}) \eta(x, y, t)$  gives

$$\frac{\partial \tilde{\eta}(\mathbf{k}, t)}{\partial t} = (k^2 - k^4 - C^2 k^2 - 2C^2 k_x^2) \tilde{\eta}(\mathbf{k}, t). \quad (9)$$

For an interface that is initially flat we set  $C = 0$  and obtain the growth rate for small fluctuations in the initial conditions:

$$\frac{\partial \tilde{\eta}(\mathbf{k}, t)}{\partial t} = k^2(1 - k^2) \tilde{\eta}(\mathbf{k}, t). \quad (10)$$

Long wavelength modes with  $k < 1$  are unstable and grow, which is exactly the instability that leads to pyramid formation. In the context of the Cahn-Hilliard equation this is the spinodal instability [8]. Note that the exponential growth of the mode is nevertheless accompanied by a decreasing total free energy, as required by Eq. (7).

For an equilibrium interface we set the slope  $C = 1$  to obtain

$$\frac{\partial \tilde{\eta}(\mathbf{k}, t)}{\partial t} = -(k^4 + k_x^2) \tilde{\eta}(\mathbf{k}, t). \quad (11)$$

The negative right hand side indicates that height fluctuations about the equilibrium slope decay, and the uniform slope profile is stable.

### III. UNCONDITIONAL VON NEUMANN STABILITY ANALYSIS

The goal in constructing a discrete time method is to be faithful to the physical behavior of the continuous time equation. In our case, this means our discrete

step should be gradient stable, to preserve the energy-decreasing property of the continuous equation. However, in this section we analyze instead von Neumann (vN) stability, i.e. the linear stability of the discrete step, Eq. (2). This analysis has certain advantages. It is relatively straightforward and, as shown in Fig. 1 and in Ref. [9], it successfully predicts the parameter range for gradient stability, as judged by numerical tests. Also, the method provides insight into the dynamics of the Fourier modes, which in the present case proves useful in clarifying the distinction between the single- and many-domain systems.

We first present vN stability analysis on the Euler step, which results in conditional stability, i.e., a lattice-dependent upper bound on  $\Delta t$ . Then we consider our parametrized semi-implicit step and perform unconditional vN stability analysis; that is, we seek parameter values which yield vN stable steps for any size  $\Delta t$ . Note that we will only impose vN stability on the equilibrium, sloped interface and not on the flat interface, where the linear instability is part of the physical behavior of the continuum equation.

In addition to the time discretization, the spatial derivatives in our equation of motion must be treated by finite-difference or spectral methods. Without specifying the details of the scheme, we denote the Fourier transform of the two-dimensional numerical laplacian as  $\lambda(\mathbf{k})$ . In the continuum limit,  $\lambda(\mathbf{k}) \rightarrow -k^2$ . For spatially discretized systems,  $0 \geq \lambda(\mathbf{k}) \geq \lambda_{\min}$ , where the value of the lower bound  $\lambda_{\min} \sim -1/\Delta x^2$  depends on the details of the discretized laplacian. Our stability conditions will rely only on the universal upper bound of zero.

We will use  $\lambda(k_x)$  to represent the Fourier transform of the numerical derivative second derivative  $\partial^2/\partial x^2$ .

#### A. Euler Step

Our discrete time step, Eq. (2), reduces to an Euler step in the case  $b_1 = b_2 = 0$ . We plug in  $h = x + \eta$  (i.e., slope  $C = 1$ ), linearize in  $\eta$ , and Fourier transform to obtain

$$\tilde{\eta}_{t+\Delta t} = \left[ 1 + \Delta t \left\{ -\lambda(\mathbf{k})^2 + 2\lambda(k_x) \right\} \right] \tilde{\eta}_t. \quad (12)$$

The vN stability condition is that the square bracket term has magnitude less than unity, to ensure fluctuations die away. The negative curly bracket term in Eq. (12) has no lower bound in the continuum limit  $\Delta x \rightarrow 0$ , and thus the Euler step would be vN unstable for any size  $\Delta t$ . The situation is improved by the numerical derivative, which places a lower bound on the curly bracket terms, leading to vN stability for  $\Delta t \lesssim |\lambda_{\min}|^{-2} \sim \Delta x^4$ . The analysis is essentially identical to what happens in the Cahn-Hilliard equation [22]. The Euler step provides an example of a lattice-dependent stability condition (relying on the lower bound of  $\lambda(\mathbf{k})$  rather than the upper bound of zero) and it results in a fixed bound on the time step, regardless of the natural time scale of the dynamics.

### B. UvN Stability for a Single Domain

We return to our parametrized discrete step, Eq. (2), but now we leave  $b_1$  and  $b_2$  unspecified. We seek to find ranges for the parameters which will lift any restrictions on  $\Delta t$ , i.e., unconditional stability. We substitute Eq. (8) with slope  $C = 1$  into Eq. (2), linearize, and Fourier transform. The resulting step can be written as

$$[1 + \Delta t \mathcal{L}(\mathbf{k})] \tilde{\eta}_{t+\Delta t} = [1 + \Delta t \mathcal{R}(\mathbf{k})] \tilde{\eta}_t \quad (13)$$

with

$$\mathcal{L}(\mathbf{k}) = b_1 \lambda(\mathbf{k}) + b_2 \lambda(\mathbf{k})^2 \quad (14)$$

and

$$\mathcal{R}(\mathbf{k}) = 2\lambda(k_x) + b_1 \lambda(\mathbf{k}) + (b_2 - 1)\lambda(\mathbf{k})^2. \quad (15)$$

Before imposing the UvN stability, we note that it is necessary to have  $\mathcal{L}(\mathbf{k}) \geq 0$  so that the square bracket on the left of Eq. (13) is non-vanishing for all  $\Delta t$  and  $\mathbf{k}$ . This gives the requirement that  $b_1 \leq 0$  and  $b_2 \geq 0$ .

Next, the UvN stability condition,  $|\tilde{\eta}_{t+\Delta t}| < |\tilde{\eta}_t|$  for all  $\Delta t$  and  $\mathbf{k}$ , will be satisfied if  $\mathcal{L}(\mathbf{k}) > |\mathcal{R}(\mathbf{k})|$ . In the case that  $\mathcal{R}(\mathbf{k})$  is positive, this gives the condition

$$0 < \mathcal{L}(\mathbf{k}) - \mathcal{R}(\mathbf{k}) = -2\lambda(k_x) + \lambda(\mathbf{k})^2, \quad (16)$$

which is intrinsically satisfied due to the non-positivity of  $\lambda(k_x)$ . While here and below the  $\mathbf{k} = 0$  mode saturates the bound, we can safely ignore it since it is static.

The crucial condition, then, comes from imposing  $\mathcal{L}(\mathbf{k}) > -\mathcal{R}(\mathbf{k})$ , which becomes

$$\lambda(k_x) + b_1 \lambda(\mathbf{k}) + \left(b_2 - \frac{1}{2}\right) \lambda(\mathbf{k})^2 > 0. \quad (17)$$

The last term is positive for  $b_2 > 1/2$ . Next, noting that  $\lambda(k_x) \geq \lambda(\mathbf{k})$ , we have a lower bound on the remaining two terms:

$$\lambda(k_x) + b_1 \lambda(\mathbf{k}) \geq (1 + b_1) \lambda(\mathbf{k}). \quad (18)$$

This will be positive provided that  $b_1 < -1$ . Thus, our conditions for UvN stability of a single-domain system are

$$b_1 < -1, \quad b_2 > 1/2, \quad (19)$$

which is plotted as the dark gray region of Fig. 1.

Note that for  $b_1$  slightly above  $-1$ , in the unstable region, it is Fourier modes with  $\lambda(k_x) \approx \lambda(\mathbf{k})$  that first violate Eq. (17). This means wavevectors  $\mathbf{k}$  that are nearly oriented along the  $x$ -axis, i.e. the gradient direction of the equilibrium interface.

### C. UvN Stability for a Many-Domain System

In a many-domain system, which is the relevant case for coarsening studies, we are not free to choose the coordinate axes to align the  $x$  axis with the interface gradient, since there are many facets with different gradient directions. To analyze this case, we first about a single domain but with an arbitrary normal direction, parametrized by the polar coordinate  $\theta$

$$h(x, y, t) = \cos(\theta)x + \sin(\theta)y + \eta(x, y, t). \quad (20)$$

This follows through just as before, with the important stability condition Eq. (17) becoming

$$\cos^2 \theta \lambda(k_x) + \sin^2 \theta \lambda(k_y) + b_1 \lambda(\mathbf{k}) + \left(b_2 - \frac{1}{2}\right) \lambda(\mathbf{k})^2 > 0. \quad (21)$$

Now, if many domains are present in the system with essentially random orientations, then for any particular Fourier mode the above equation will be averaged over  $\theta$ , giving  $\langle \cos^2 \theta \rangle = \langle \sin^2 \theta \rangle = 1/2$ . Using

$$\lambda(k_x) + \lambda(k_y) \approx \lambda(\mathbf{k}) \quad (22)$$

reduces Eq. (21) to

$$\left(b_1 + \frac{1}{2}\right) \lambda(\mathbf{k}) + \left(b_2 - \frac{1}{2}\right) \lambda(\mathbf{k})^2 > 0. \quad (23)$$

Thus, our UvN stability condition for many-domain systems is

$$b_1 < -1/2, \quad b_2 > 1/2, \quad (24)$$

which is depicted as the combined shaded regions of Fig. 1. The averaging over multiple orientations provides a greater parameter range of stability than the single-domain case.

Note that in general Eq. (22) is only an approximate relationship. It is a strict equality in the  $\Delta x \rightarrow 0$  continuum limit, and also in the common five-point stencil for the numerical laplacian on a square lattice, but for other choices of numerical derivatives it need not be exact.

## IV. NUMERICAL TESTS OF GRADIENT STABILITY

Since the field equation of motion is nonlinear, von Neumann stability analysis is not sufficient to prove gradient stability. For that reason, we have conducted extensive numerical tests for gradient stability for a range of  $b_1$  and  $b_2$  parameter values. We present the details of the numerical derivative implementation in an appendix, but we note here two important general features such an implementation should have. First, the local conservation law should be constructed to hold exactly, not just to some order in  $\Delta x$ , and second, the energy-decay

property of the continuous time equation should be maintained when spatially discretizing. That is, the particular scheme of calculating the spatially discrete analog of the free energy  $F[h]$  in Eq. (6) and the equation of motion should be consistent, so that

$$\frac{d}{dt}\phi_{ij} = -\frac{\partial F}{\partial \phi_{ij}} \quad (25)$$

is an exact relation, not just approximate to some order in  $\Delta x$ .

For each  $b_1$  and  $b_2$  value represented as a data point in Fig. 1 we performed the following tests. We evolved a  $512 \times 512$  sized lattices with lattice constant  $\Delta x = 1$  out to a final time  $t_{\max}$ . These systems were evolved using three different methods: an Euler step with  $\Delta t = 0.03$  out to a  $t_{\max} = 10^4$ , a semi-implicit step with  $b_1 = 2.5$  and  $b_2 = 1$  and growing time step  $\Delta t = 0.03t^{2/3}$  out to time  $t_{\max} = 10^6$ , and the same semi-implicit parameters with a fixed time step  $\Delta t = 100$  out to time  $t_{\max} = 10^6$ . For each of these cases we analyzed multiple runs and varied between random initial conditions and sinusoidal initial conditions with long and short wavelengths.

At regular intervals during the evolution we tested a single step calculated via Eq. (2) with sizes varied between  $1 \leq \Delta \leq 10^{10}$ . This step was used only for energy stability testing and did not contribute to the subsequent time evolution. Any time that the free energy was found to increase, that particular set of parameter values was identified as unstable.

For the many-domain system, we used periodic boundary conditions and an initially flat interface (plus the random or sinusoidal fluctuations). For the single-domain system, we first re-write the field equation of motion, Eq. (1) in terms of deviations from the uniform slope, giving

$$\begin{aligned} \frac{\partial \eta}{\partial t} = & -\nabla^4 \eta + 2\partial_x^2 \eta + 2\partial_x |\nabla \eta|^2 + 2(\partial_x \eta) \nabla^2 \eta \\ & + \nabla \cdot (|\nabla \eta|^2 \nabla \eta), \end{aligned} \quad (26)$$

where  $\partial_x = \partial/\partial x$ , and then constructed the analogous numerical implementation of this equation. This approach was necessary to eliminate sensitivity to truncation error. We imposed periodic boundary conditions on  $\eta$ , which corresponds to shifted periodic boundary condition on  $h$ .

In Fig. 1 we show the results of this testing both for the single- and many-domain systems. The (blue) circles represent parameter values that were found to be stable for the single-domain system, that is, under all our testing, there were no single incidents of energy increase. The (purple) squares are parameters values that were found to be unstable in the single-domain system, but stable for the many-domain case. The remaining  $\times$  are parameter values found to be unstable for both single- and many-domain systems. We find a striking degree of agreement between the predictions of UvN stability analysis and the numerical tests for unconditional gradient stability. This is one of our main results.

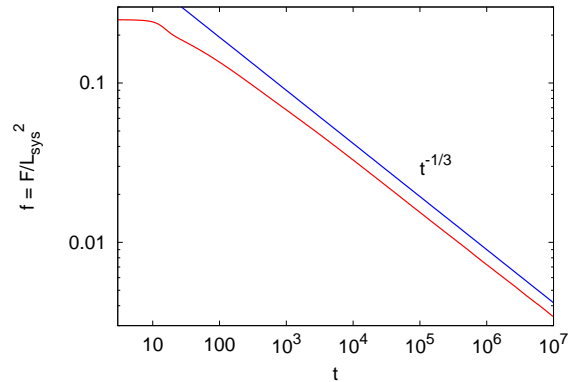


FIG. 2. (color online) The free energy density  $f = F[h]/L_{\text{sys}}^2$  as a function of time, where the time evolution utilized a growing time step,  $\Delta t \sim t^{2/3}$ . Simulation details are in the text. The expected  $t^{-1/3}$  decay is plotted for comparison.

There is a small region for  $b_2 < 1/2$  where numerical tests find gradient stability. This can be understood from Eq. (17) as a lattice-dependent stability arising from the laplacian lower bound  $\lambda_{\min}$ . We have emphasized instead the lattice-independent stability boundaries, as these are more widely applicable.

To illustrate the utility of these methods, we have simulated the coarsening that results from an initially flat interface, using a the stable step parameters  $b_1 = -1.5$  and  $b_2 = 1$  and a growing step size  $\Delta t = \max(0.1, 0.01t^{2/3})$ . We performed 20 independent runs on a  $2048 \times 2048$  lattice with  $\Delta x = 1$ , out to time  $t_{\max} = 10^7$ .

Fig. 2 shows the decay of the free energy with time. Once equilibrated domains form, the free energy density  $F$  is proportional to the amount of edge in the system, which is inversely proportional to the characteristic size of the domains. Thus the free energy should decay as  $F \sim 1/L(t) \sim t^{-1/3}$ . Our growing time step integration reproduces this result.

Shown in Fig. 3 are snapshots of domain configurations for various times from a single run on a  $512 \times 512$  lattice, with all other parameters as given above.

## V. SUMMARY

We have parametrized a first order accurate discrete time step, Eq. (2) for MBE growth with slope selection that, unlike the Euler step, is gradient stable for appropriate choices of the parameters  $b_1$  and  $b_2$ . We determined the stability range for these parameters via unconditional von Neumann stability analysis, and then tested these predictions with numerical tests for gradient stability, as shown in Fig. 1. We find that the UvN stability analysis serves as an accurate proxy for unconditional gradient stability, similar to the behavior of the Cahn-Hilliard equation [9].

Our stability analysis contained an implicit assumption

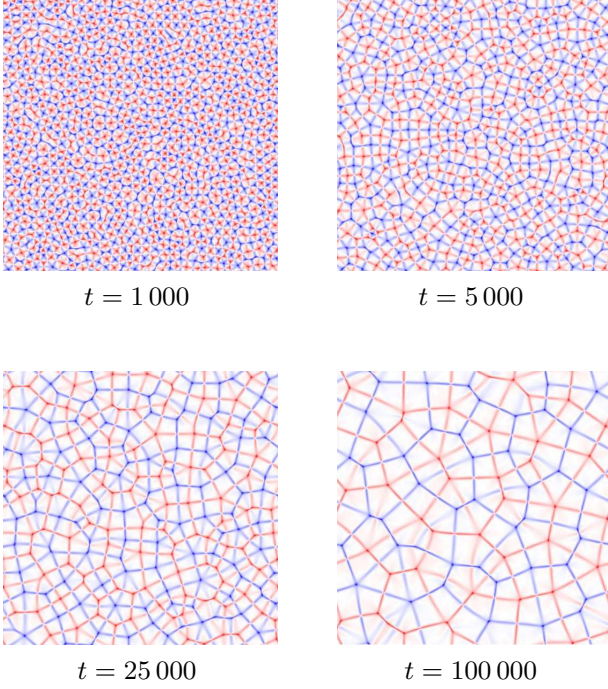


FIG. 3. (color online) Plotted is the laplacian of  $h(x, y, t)$ , for a system evolved with a growing time step  $\Delta t \sim t^{2/3}$ . Simulation details are provided in the text. Positive values (troughs) are red, negative values (peaks) are blue, and the white regions are domains of uniform slope with zero laplacian.

that the interface slopes do not exceed unit magnitude, which we justify by noting that the dynamics naturally select for this slope. This came into our UvN analysis by our choice to linearize about a unit slope domain. We note that the numerical tests for gradient stability contained no such assumption, so the agreement between the two approaches confirms validity of the unit slope assumption.

Since UvN stability analysis is a relatively straightforward process, we expect this approach to be generally applicable to a wide variety of phase field models. In particular, the case of slope-selecting MBE growth with preferred slope orientations, as studied by [5, 16, 23, 24] and others, should follow identically to the case presented here.

## ACKNOWLEDGMENTS

G.M.S. was supported by NSF REU Grant PHY-1156964. B.P.V.-L. acknowledges financial support from the Max Planck Institute for Dynamics and Self-Organization and the hospitality of the University of Göttingen, where this work was completed.

## Appendix: Finite Difference Scheme

Here we present details of the spatial discretization scheme we used in our numerical tests. We present these in a discrete-space, continuous time picture, as our goal is to ensure that the conservative dynamics and the gradient flow are exact, i.e. preserved to all orders in  $\Delta x$ . The essential condition for gradient flow is that the equation of motion must be connected to a particular choice for the free energy functional such that

$$\frac{\partial h_{i,j}}{\partial t} = -\frac{\partial}{\partial h_{i,j}} \left( \frac{F}{\Delta x^2} \right). \quad (\text{A.1})$$

Local conservation is imposed by ensuring that the equation of motion has the form

$$\frac{dh_{i,j}}{dt} = -\frac{1}{\Delta x} \left[ \{J_x\}_{i+1/2,j} - \{J_x\}_{i-1/2,j} - \{J_y\}_{i,j+1/2} - \{J_y\}_{i,j-1/2} \right] \quad (\text{A.2})$$

so that the same  $\{J_x\}_{i+1/2,j}$  flows into  $h_{i+1,j}$  and out of  $h_{i,j}$ , and the same  $\{J_y\}_{i,j+1/2}$  flows into  $h_{i,j+1}$  and out of  $h_{i,j}$ .

Our implementation uses an on-site finite-difference expression for  $\nabla^2 h$ , for which we take the standard five-point stencil,

$$\{\nabla^2 h\}_{i,j} = \frac{1}{\Delta x^2} [h_{i+1,j} + h_{i-1,j} + h_{i,j+1} + h_{i,j-1} - 4h_{i,j}], \quad (\text{A.3})$$

and the cell-centered expression for  $|\nabla h|^2$ ,

$$\begin{aligned} \{|\nabla h|^2\}_{i+1/2,j+1/2} = & \frac{1}{2\Delta x^2} \left[ (h_{i+1,j} - h_{i,j})^2 + (h_{i+1,j+1} - h_{i,j+1})^2 \right. \\ & \left. + (h_{i,j+1} - h_{i,j})^2 + (h_{i+1,j+1} - h_{i+1,j})^2 \right]. \end{aligned} \quad (\text{A.4})$$

With these choices it is straightforward to show that

$$\frac{\partial}{\partial h_{k,l}} \sum_{i,j} \{|\nabla h|^2\}_{i+1/2,j+1/2} = -2\{\nabla^2 h\}_{k,l}. \quad (\text{A.5})$$

Our equation of motion is given by Eq. (A.1) with the choice

$$\frac{F}{\Delta x^2} = \sum_{i,j} \left[ \frac{1}{2} \{\nabla^2 h\}_{i,j}^2 + \frac{1}{4} \left( 1 - \{|\nabla h|^2\}_{i+1/2,j+1/2} \right)^2 \right]. \quad (\text{A.6})$$

By making use of Eq. (A.5), the equation of motion can be shown to satisfy the discrete continuity equation (A.2) with current

$$\{J_x\}_{i+1/2,j} = \{J_x^{SD}\}_{i+1/2,j} + \{J_x^{NE}\}_{i+1/2,j} \quad (\text{A.7})$$

where the surface diffusion current is

$$\{J_x^{SD}\}_{i+1/2,j} = \frac{\{\nabla^2 h\}_{i+1,j} - \{\nabla^2 h\}_{i,j}}{\Delta x}, \quad (\text{A.8})$$



and the nonequilibrium current is

$$\{J_x^{NE}\}_{i+1/2,j} = \frac{h_{i+1,j} - h_{i,j}}{\Delta x} \times \left[ 1 - \frac{1}{2} \left( \{|\nabla h|^2\}_{i+1/2,j+1/2} + \{|\nabla h|^2\}_{i+1/2,j-1/2} \right) \right], \quad (\text{A.9})$$

and analogous expressions for  $\{J_y\}_{i,j+1/2}$ . The discrete form of the free energy, Eq. (A.6), was used in all our numerical tests for gradient stability.

- 
- [1] G. Ehrlich and F. G. Hudda, J. Chem. Phys. **44**, 1039 (1966)
  - [2] R. L. Schwoebel and E. J. Shipsey, J. Appl. Phys. **37**, 3682 (1966)
  - [3] J. Villain, J. Phys. I France **1**, 19 (1991)
  - [4] M. Ortiz, E. Repetto, and H. Si, J. Mech. Phys. Solids **47**, 697 (1999)
  - [5] D. Moldovan and L. Golubovic, Phys. Rev. E **61**, 6190 (2000)
  - [6] C. Wang, X. Wang, and S. M. Wise, Discrete Cont. Dyn. S. **28**, 405 (2010)
  - [7] R. V. Kohn and X. Yan, Comm. Pure App. Math. **56**, 1549 (2003)
  - [8] A. J. Bray, Adv. Phys. **43**, 357 (1994)
  - [9] B. P. Vollmayr-Lee and A. D. Rutenberg, Phys. Rev. E **68**, 066703 (2003)
  - [10] M. Cheng and A. D. Rutenberg, Phys. Rev. E **72**, 055701 (2005)
  - [11] D. J. Eyre, MRS Proceedings **529**, 39 (1998)
  - [12] J. Shen, C. Wang, X. Wang, and S. M. Wise, SIAM J. Numer. Anal. **50**, 105 (2012)
  - [13] Z. Qiao, Z.-z. Sun, and Z. Zhang, Numer. Methods for Partial Differential Eq. **28**, 1893 (2012)
  - [14] W. Chen and Y. Wang, Numer. Math. **122**, 771 (2012)
  - [15] W. Chen, C. Wang, X. Wang, and S. Wise (preprint)
  - [16] C. Xu and T. Tang, SIAM J. Numer. Anal. **44**, 1759 (2006)
  - [17] B. P. Vollmayr-Lee (in preparation)
  - [18] W. W. Mullins, J. Appl. Phys. **30**, 77 (1959)
  - [19] M. D. Johnson, C. Orme, A. W. Hunt, D. Graff, J. Sudijono, L. M. Sander, and B. G. Orr, Phys. Rev. Lett. **72**, 116 (1994)
  - [20] M. Siegert and M. Plischke, Phys. Rev. Lett. **73**, 1517 (1994)
  - [21] M. Rost and J. Krug, Phys. Rev. E **55**, 3952 (1997)
  - [22] T. M. Rogers, K. R. Elder, and R. C. Desai, Phys. Rev. B **37**, 9638 (1988)
  - [23] M. Siegert, Phys. Rev. Lett. **81**, 5481 (1998)
  - [24] S. J. Watson and S. A. Norris, Phys. Rev. Lett. **96**, 176103 (2006)